

The physiological plausibility of time-varying Granger-causal modeling: Normalization and weighting by spectral power



Gijs Plomp^{a,*}, Charles Quairiaux^a, Christoph M. Michel^{a,b}, Laura Astolfi^{c,d}

^a Functional Brain Mapping Laboratory, Department of Fundamental Neuroscience, University of Geneva, Geneva, Switzerland

^b Neurology Clinic, University Hospital Geneva, Switzerland

^c Department of Computer, Control, and Management Engineering, University of Rome "Sapienza", Italy

^d Santa Lucia Foundation IRCCS, Rome, Italy

ARTICLE INFO

Article history:

Accepted 4 April 2014

Available online 13 April 2014

Keywords:

Barrel cortex

Dynamics

EEG

Effective connectivity

Functional networks

Granger causality

ABSTRACT

Time-varying connectivity methods are increasingly used to study directed interactions between brain regions from electrophysiological signals. These methods often show good results in simulated data but it is unclear to what extent connectivity results obtained from real data are physiologically plausible. Here we introduce a benchmark approach using multichannel somatosensory evoked potentials (SEPs) measured across rat cortex, where the structural and functional connectivity is relatively simple and well-understood. Rat SEPs to whisker stimulation are exclusively initiated by contralateral primary sensory cortex (S1), at known latencies, and with activity spread from S1 to specific cortical regions. This allows for a comparison of time-varying connectivity measures according to fixed criteria. We thus evaluated the performance of time-varying Partial Directed Coherence (PDC) and the Directed Transfer Function (DTF), comparing row- and column-wise normalization and the effect of weighting by the power spectral density (PSD). The benchmark approach revealed clear differences between methods in terms of physiological plausibility, effect size and temporal resolution. The results provide a validation of time-varying directed connectivity methods in an animal model and suggest a driving role for ipsilateral S1 in the later part of the SEP. The benchmark SEP dataset is made freely available.

© 2014 Elsevier Inc. All rights reserved.

Introduction

Sensory, cognitive and motor processing consists of dynamically coordinated activity in functional networks of brain regions. In such large-scale networks the activity in one region may drive activity in other regions, and which regions drive one another varies with time and task. A better understanding of directed interactions and their dynamics may help to better comprehend sensory and cognitive processing in both health and disease (Bressler and Seth, 2011; Bressler, 1995). Reliable time-varying methods are therefore needed that can identify from electrophysiological signals what the important drivers of cortical networks are, which regions they most strongly drive to, and how driving from each region varies with time.

Various time-varying methods exist that can model directed interactions from non-stationary electrophysiological recordings (Astolfi et al., 2008; Ding et al., 2000; Hesse et al., 2003; Hu et al., 2012; Lin et al., 2009; Milde et al., 2010; Porcaro et al., 2013; Sommerlade et al., 2012; van Mierlo et al., 2011; Wilke et al., 2007). Such methods may correctly represent directed interactions in simulated data but when applied to human data it is often unclear

whether connectivity results correctly reflect the underlying physiology. This is because EEG and MEG signals at each electrode or source point reflect activity from multiple regions to unknown extents: the problem of volume conduction (Gómez-Herrero et al., 2008; Haufe et al., 2013; Nolte et al., 2004; Nunez and Srinivasan, 2006). In addition, large-scale human functional connectivity and its dynamics are not well-understood so that connectivity results cannot be easily compared to the underlying physiology, even in intracranial recordings.

We here use multichannel electrophysiological recordings from rats as a benchmark to test the performance of directed, time-varying connectivity methods. In rat cortex structural and functional connectivity are simpler than in human, and better understood because more direct electrophysiological measures are possible in animal models. After unilateral whisker stimulation the spatiotemporal dynamics of evoked activity follows a known pattern that reflects the underlying structural connectivity (Quairiaux et al., 2011). Rat SEPs can therefore provide a good benchmark to evaluate results from time-varying connectivity estimators, for three reasons in particular. Firstly, the SEP is entirely driven by the primary sensory cortex contralateral (cS1) to whisker stimulation (Farkas et al., 1999; Shuler et al., 2001). Secondly, activity in cS1 is known to start at around 5 ms after whisker stimulation and ceases at around 25 ms, as shown by intracranial recordings in anesthetized animals (Armstrong-James et al., 1992; Constantinople and Bruno, 2013; Quairiaux et al., 2011).

* Corresponding author at: University of Geneva, Dept. of Fundamental Neuroscience, Functional Brain Mapping Lab., Rue Michel-Servet 1, CH-1211 Geneva, Switzerland.
E-mail address: Gijs.Plomp@unige.ch (G. Plomp).

Outside these latencies driving from cS1 to other regions is physiologically not plausible. Thirdly, cS1 has structural connections to specific regions in both hemispheres (Colechio and Alloway, 2009; Hoffer et al., 2003; Lee et al., 2011; Smith and Alloway, 2013; Zakiewicz et al., 2011). In line with structural connectivity, contralateral parietal and frontal sensory-motor regions become active immediately after cS1 (see Fig. 1, dark blue and orange traces).

Out of the numerous published Granger-causal methods we here selected time-varying PDC and DTF for comparison (Kaminski and Blinowska, 1991; Baccalá and Sameshima, 2001; Astolfi et al., 2008). These methods, based on multivariate autoregressive modeling, are variations within the Wiener–Granger causality theoretic framework, quantifying how activity at one region predicts activity at other regions (Bressler and Seth, 2011; Granger, 1969).

PDC is a linear multivariate method that separates direct from indirect connections and can correctly identify interactions even in relatively noisy data (Astolfi et al., 2006, 2007b; Baccalá and Sameshima, 2001; Fasoula et al., 2013; Florin et al., 2011). Stability and interpretability of PDC results are achieved through normalization. The original PDC definition normalizes the outgoing connection strengths from each region, a *column-wise* normalization that bounds the sum of the outflows per region to one (Baccalá and Sameshima, 2001). This bounding however,

may compromise the sensitivity to outflows and therefore a normalization by inflows may be preferred. This row-wise normalization is part of the original DTF definition and has also been applied to PDC (Astolfi et al., 2007a; Kaminski and Blinowska, 1991; Kus et al., 2004). Row-wise normalized methods may be advantageous in studying neural systems because they allow more variability in outgoing connection strengths, but to our knowledge a direct comparison of the effects of row- and column-wise normalizations in real data is so far missing.

PDC is a measure in the frequency domain that quantifies to what degree a power change at frequency f predicts a power change in another region at f . That is, PDC represents a directional *rate of change* in the spectral power between two regions: large PDC_{ij} indicates that increased spectral power in the source region yields a large increase in the destination region (Schelter et al., 2009). However, the PDC calculation is independent of the signal spectral power, and therefore large PDC can occur from regions that show little spectral power, and vice versa. PDC values therefore lack a clear physiological interpretation (Baccalá and Sameshima, 2001; Faes et al., 2012). To increase the physiological interpretability we weigh PDC values by the instantaneous power spectral density (PSD) in the source region. This weighting reflects the fact that activity in a source region is necessary, but not sufficient, in order for the source region to effectively drive activity in

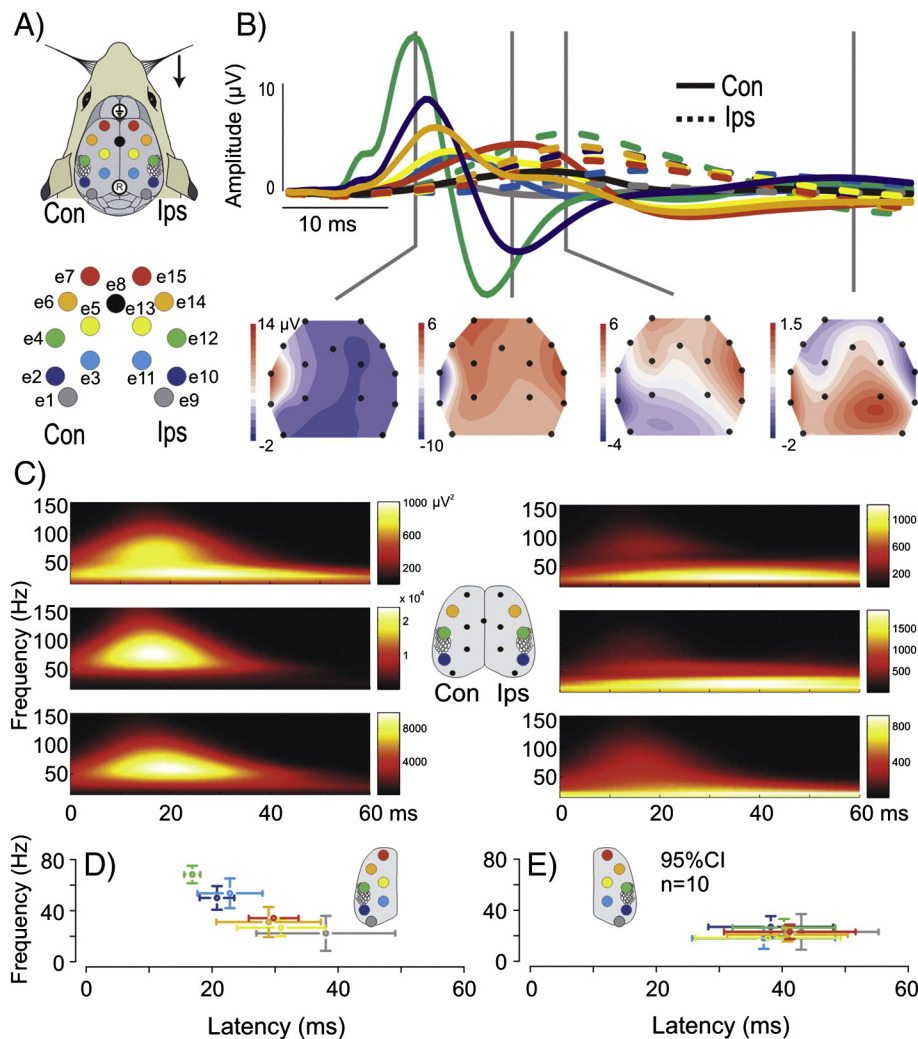


Fig. 1. Large-scale SEP mapping after whisker stimulation (A) A multi-electrode grid placed on the skull bone recorded unilateral SEPs across cortex. The hemisphere contralateral (Con) to stimulation is shown on the left, ipsilateral (Ips) on the right. The electrode layout is shown below with color-coding used in all plots. (B) In the grand-average SEP ($n = 10$), the maximum voltage peak over cS1 (e4, dark green; mean 13.9 ms, 95% bootstrapped confidence intervals (CI) 13.1–14.9 ms) was quickly followed by peak activity over more parietal (e2, dark blue; 15.4 ms, CI 14.2–16.2 ms), frontal areas (e6, orange; 15.6 ms, CI 14.4–16.4 ms). At middle latencies the maximal activity was measured over iS1 (e12, green dotted line; 29.0 ms, CI 26.5–31.4 ms). Topographic layouts of the voltage potential (2D spline interpolation) are plotted below to illustrate large-scale activity spread. (C) Shows time-frequency plot of the SEP for three nearby electrodes. (D) Latency (ms) vs. Frequency (Hz) plot showing peak latencies for different electrodes. (E) Latency (ms) vs. Frequency (Hz) plot showing 95% CI for $n=10$.

other regions. Similar spectral weightings have been previously proposed for PDC (Takahashi et al., 2010) and for DTF (Van Mierlo et al., 2011, 2013). Here we systematically evaluate the effect of spectral weighting on connectivity results for both PDC and DTF. We compared a total of four PDC implementations (column-wise normalized PDC, row-wise normalized PDC, column-wise normalized weighted PDC (wPDC), and row-wise normalized wPDC) and two DTF implementations (an unweighted and a spectrally weighted one).

Like PDC, DTF is a linear, multivariate implementation of Granger-causality defined in the frequency domain, but using a row-wise normalization (Kaminski and Blinowska, 1991; Kus et al., 2004). In contrast to PDC, DTF does not distinguish between direct and indirect interactions; it quantifies the total driving of a region on the entire network, irrespective of the routing of that influence through other regions.

We compared connectivity results of these methods in multichannel SEP data recorded across rat cortex according to three performance criteria: 1) Can cS1 be identified as the initial main driver, and how well; 2) Are the peak latencies of cS1 driving physiologically plausible; and 3) Does early cS1 driving specifically target contralateral parietal and frontal regions? These criteria clearly differentiated between the tested methods. Results closest to what may be expected from physiology were obtained with row-normalized wPDC and wDTF. In addition to showing the feasibility of a benchmark approach in real data, the results also showed strong indications that ipsilateral S1 is an important network driver at longer latencies.

Material and methods

All animal handling procedures were in accordance with Swiss Federal laws. We analyzed data of 10 young Wistar rats (P21; half were male) from previously published work (Quairiaux et al., 2011). While the animals were under light isoflurane anesthesia, multichannel epicranial EEG was recorded from a grid of 16 stainless steel electrodes placed directly on the skull bone, covering the entire cortex (Fig. 1A). The EEG was filtered online between 1 and 500 Hz and sampled at 2 kHz. Unilateral SEPs were recorded by presenting 50 right- and 50 left-sided whisker stimulations in separate blocks. The inter-stimulus interval was 9 s. For further details, see (Quairiaux et al., 2011).

We calculated SEPs by averaging responses per animal and condition (left, right). We combined results within animals for left and right stimuli, representing them as responses to contralateral and ipsilateral stimuli.

Time-varying Granger-causal modeling

PDC quantifies the predictability between multiple pairs of signals based on the concept of Granger causality (Baccalá and Sameshima, 2001; Bressler and Seth, 2011; Granger, 1969). This states that a time series s_1 can be said to cause another time series s_2 if knowledge of past samples of s_1 reduces the prediction error for the present sample of s_2 , i.e. if activity in s_1 predicts s_2 .

The predictability of s_2 by past samples of s_1 can be quantified through simultaneous multivariate autoregressive (MVAR) modeling of the N signals in S :

$$S(t) = [S_1(t), S_2(t), \dots, S_N(t)]^T. \quad (1)$$

We assume the following MVAR process to adequately describe the data:

$$\sum_{k=0}^p A_k S(t-k) = E(t). \quad (2)$$

Here $S(t)$ is the data vector in time, $E(t)$ is a vector of multivariate zero-mean uncorrelated white noise processes, A_k is the $N \times N$ matrix

of model coefficients at lag k , and p is the model order, determining the size of the prediction window. To avoid volume conduction effects in the analysis the cross-coefficients at zero lag are set to zero, so that A_0 is equal to identity matrix I .

MVAR modeling separates direct and indirect influences between s_1 and s_2 by discounting the cascade effects from s_1 onto s_2 mediated by other time-series. This way $A(k)$ between two signals reflects only the direct interactions between regions.

We derived time-varying connectivity estimators using adaptive MVAR (AMVAR) models (Astolfi et al., 2008; Hesse et al., 2003). This approach makes no assumptions about the stationarity of the signal, contrary to the classic MVAR approach. We estimated time-dependent parameter matrices $A(k, t)$ by means of a Recursive Least Squares (RLS) algorithm with a forgetting factor (Hesse et al., 2003). RLS minimizes the sum of exponentially weighted prediction errors of the processes' past. The weighting depends on an adaptation constant (typically 0.01–0.04, Astolfi et al., 2008) which controls the trade-off between adaptation speed and quality of estimation. Values close to zero result in slower adaptation and more stable estimations, and vice versa. Here we used an adaptation constant of 0.02, suggested by simulation studies for the comparable levels of Signal to Noise Ratio (SNR) and amount of trials. A full description of the RLS algorithm can be found elsewhere (Hesse et al., 2003; Möller et al., 2001).

To arrive at a spectral representation, Eq. (2) is transformed to the frequency domain at every time-point:

$$A(f, t)S(f, t) = E(f, t) \quad (3)$$

where

$$A(f, t) = \sum_{k=0}^p A_k(t) e^{-j2\pi f \Delta t k} \quad (4)$$

with Δt being the temporal interval between successive samples.

The PDC is then classically defined by a column-wise normalization, i.e. a normalization with respect to outgoing connection strengths (Baccalá and Sameshima, 2001):

$$\text{sPDC}_{ij}(f, t) = \frac{|A_{ij}(f, t)|^2}{\sum_{m=1}^N |A_{mj}(f, t)|^2}. \quad (5)$$

Where we squared the PDC values (sPDC) to further enhance accuracy and stability (Astolfi et al., 2006). The corresponding row-wise normalization, i.e. a normalization with respect to incoming connection strengths is then:

$$\text{sPDC}_{ij}(f, t) = \frac{|A_{ij}(f, t)|^2}{\sum_{m=1}^N |A_{im}(f, t)|^2}. \quad (6)$$

Using the transfer matrix H of the AMVAR model (Eq. 3) DTF is defined as:

$$\text{DTF}_{ij}(f, t) = \frac{|H_{ij}(f, t)|^2}{\sum_{m=1}^N |H_{im}(f, t)|^2}. \quad (7)$$

We calculated time-varying PDC and DTF values using non-averaged single sweeps between -10 and 60 ms around stimulus onset. For each trial we automatically chose the model order p using the Akaike Information Criteria (AIC) for MVAR processes. The average model order p was 8 time frames (4 ms). We then calculated median time-

varying connectivity values per animal and stimulation condition (left/right).

Spectral weighting

We weighted PDC by the PSD at each source region, defining a weighted PDC (wPDC):

$$\text{wPDC}_{ij}(f, t) = \text{sPDC}_{ij}(f, t) \cdot S_j(f, t) \quad (8)$$

where S_j is the PSD at the source region.

Before weighting, we computed PSD on single-trials between -120 and 120 ms around stimulus onset using the S-transform (Stockwell et al., 1996) and then averaged it for each animal and condition (left, right). The bin size of the S-transform was 5.5 Hz. Average PSD was then scaled (0–1) across electrodes, time (0 to 60 ms) and frequencies (1–150 Hz). PDC values were similarly scaled before multiplication (Eq. 7). Since wPDC is the product of PDC and PSD, wPDC values range between 0 and 1. Due to this scaling, $\text{wPDC}_{(ij)}(f, t)$ is 1 only when the PSD maximum occurs in the same region as the maximum PDC, and at the same frequency and latency. When either PDC or PSD is low, wPDC will also be low. The same holds for spectrally weighted DTF (wDTF), which was computed analogous to wPDC, following Eq. 8.

Time-varying connectivity values were calculated within animal and per stimulation condition (left, right). We then averaged for each animal the directed connectivity matrices for left and right stimuli in order to represent them as responses to contralateral and ipsilateral stimuli, respectively.

Frequency of interest selection

The spectral analysis of the evoked response showed that the dominant frequencies strongly depended on electrode and stimulated side (Fig. 1D–E). To account for this frequency specificity we identified

the frequency of maximal PSD at each electrode and time-point as the frequency of interest. We further analyzed connectivity results at these frequencies only. This data-driven approach reduces the dimensionality of the results and assures that for each electrode and stimulation condition the dominant frequencies are taken into account. The approach is illustrated for column- and row-wise normalized PDC in Fig. 2.

Statistics

To statistically compare the summed driving from a region, or the directional specificity of driving, we calculated 95% CIs of within-animal differences using non-parametric bootstrapping ($n = 10,000$) across animals, with the null-hypothesis of no difference between conditions or directions, respectively. We used a non-parametric approach since normality cannot always be assumed with small sample sizes (our $n = 10$). We used a similar bootstrapping procedure to compute 95% CIs around the mean values for plotting purposes.

To compare results across methods we calculated effect sizes for each statistical comparison using Cohen's d with pooled s.d.s in the denominator (Cohen, 1992). The effect size quantifies the difference between two observed means relative to the standard deviation, providing a way to compare effects across measures or studies.

Results

The first performance criterion was whether cS1 could be distinguished as the main driver at early latencies, and how well. We summed per region the outgoing connection strengths to all other regions (outflows) as a measure of the total driving of each region onto the network. The time-series of total driving for the six methods are shown in Fig. 3. Each method except unweighted DTF identified cS1 (e4, in green) as the largest driver at short latencies after stimulation. For column-

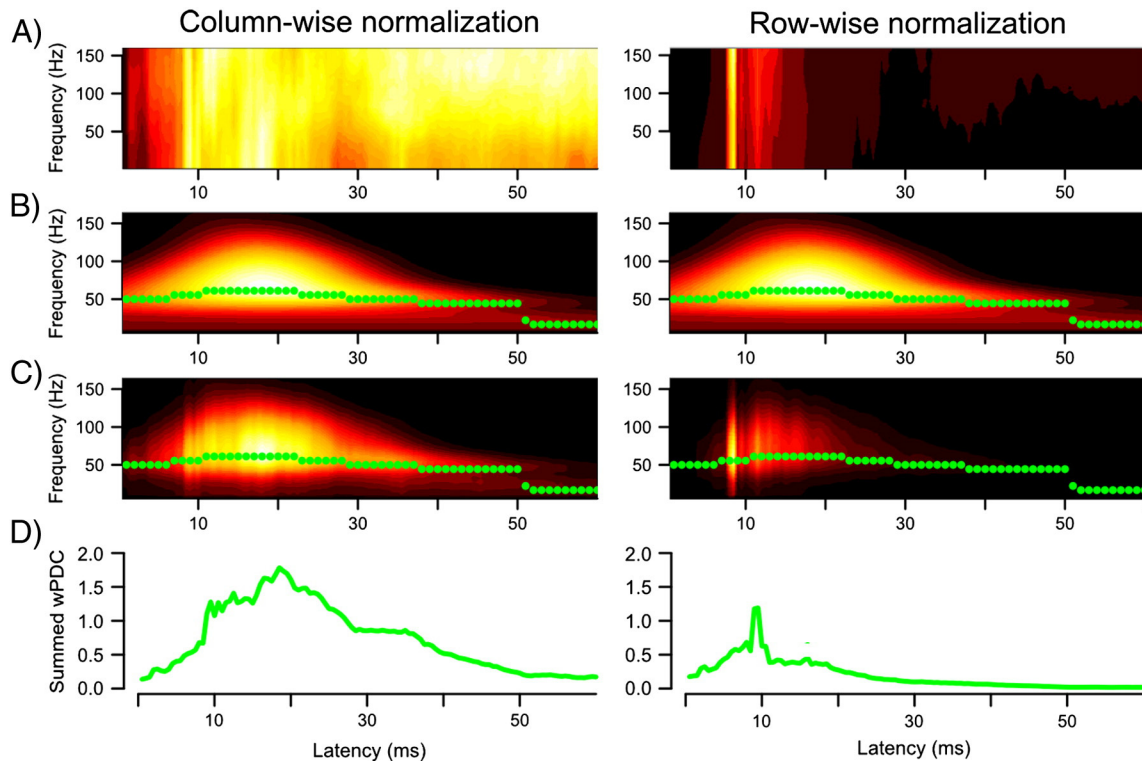


Fig. 2. Weighting and frequency selection example. A) Shows time-frequency plot of summed PDC from cS1 for column-wise normalization (left) and row-wise normalization (right). Averaged data from one animal (IC070523). B) Shows the broadband PSD in cS1 with the frequency of instantaneous maximal PSD indicated by the green dots. C) Shows the time-frequency plot of summed wPDC. The summed wPDC at the frequency of maximal PSD is shown in D).

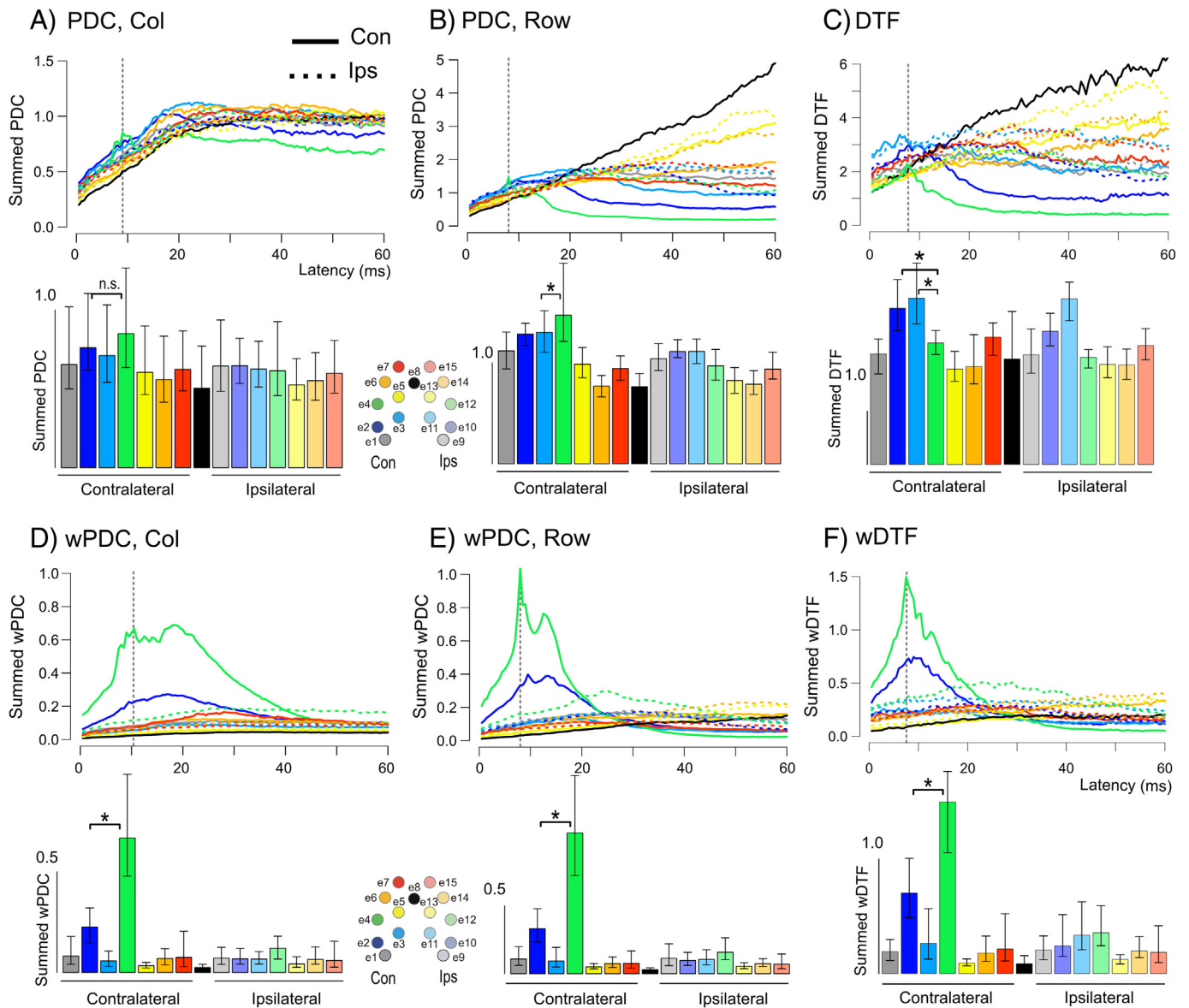


Fig. 3. Dynamics of summed driving and discriminability of cS1 for each method. The summed grand-average (w)PDC and (w)DTF time-series for each contralateral and ipsilateral electrode, colors as in Fig. 1. Early peak latencies of cS1 driving are indicated by vertical gray dotted lines. Barplots are drawn at the peak latencies indicated by gray dotted lines and show average summed outflows for each electrode with error bars denoting bootstrapped 95% CI around the mean across animals ($n = 10$).

normalized PDC the peak driving from cS1 did not significantly differ from that of the second-largest driver (e2, dark blue; lower 95% confidence interval (CI) of bootstrapped pairwise differences smaller than 0). Row-normalized PDC showed significantly larger driving from cS1 than from the second-largest driver (e3, light blue); column- and row-normalized wPDC, as well as wDTF showed significantly larger driving from cS1 than from the second-largest driver (e2). The effect sizes for distinguishing cS1 from the second-largest driver are listed in Table 1, indicating that cS1 driving was most clearly identified by wPDC and wDTF.

Table 1
Effect sizes (d) for cS1 identification.

	PDC column-normalized	PDC row-normalized	DTF
Plain	0.2	0.3	n.a.
Weighted	1.4	1.5	1.5

The second performance criterion was whether peak driving from cS1 occurred at physiologically plausible latencies, roughly between 5 and 25 ms after stimulus onset. Table 2 shows the average latencies and 95% CIs of peak driving from cS1. Each method correctly identified latencies close to the peak amplitudes of the ERP (13.9 ms, 95% CI 13.1–14.9 ms), at which there is considerable neural activity in cS1 (Armstrong-James et al., 1992; Constantinople and Bruno, 2013; Quairiaux et al., 2011). For row-normalized PDC and DTF the 95% confidence intervals were about half the size as compared to column-normalized methods, which more closely reflected the 2 ms 95% CI of the peak ERP latencies at cS1 (Fig. 1).

Table 2
Peak latencies of driving from cS1 for each method.

	PDC column-normalized	PDC row-normalized	DTF
Plain	10.3 (8.8–13.9)	8.9 (8.2–10.5)	8.4 (7.9–9)
Weighted	13.4 (11.1–16.1)	8.9 (8.2–10.6)	8.8 (8.0–10.7)

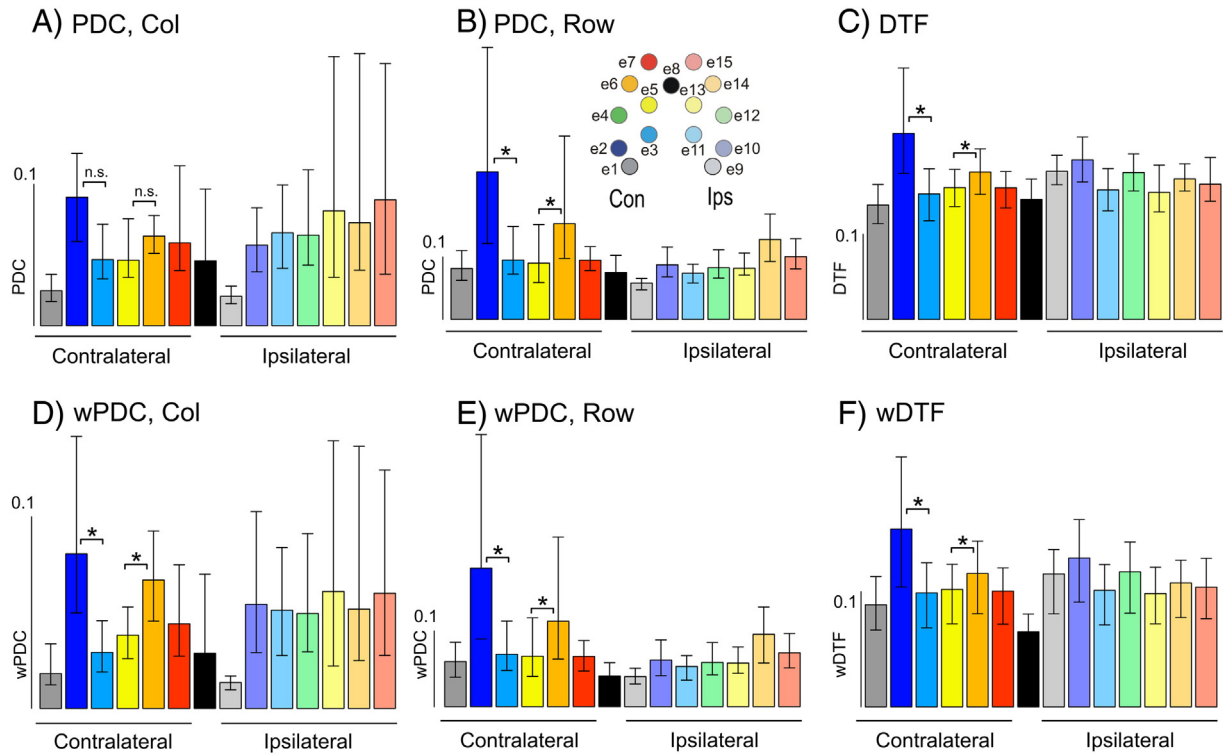


Fig. 4. Directions of driving from contralateral S1. Barplots show the driving from cS1 to all target regions in the hemisphere contralateral and ipsilateral to stimulation, for each method. Barplots are drawn at latencies corresponding to the peak latencies in Fig. 3. Error bars denote 95% CI around the mean.

The third performance criterion was whether early driving from cS1 specifically targets parietal (e2) and sensory-motor (e6) regions. These two regions show significant activation shortly after cS1 (Quairiaux et al., 2011) and receive direct structural connections from S1 (Hoffer et al., 2003; Lee et al., 2011; Smith and Alloway, 2013; Zakiewicz et al., 2011). The directional specificity of driving from cS1 is depicted in Fig. 4 per method. All methods correctly identified e2 and e6 as the main targets of cS1 driving. We statistically compared cS1 driving to e2 and to e6 with that toward medial electrodes equidistant from cS1, e3 and e5 respectively. These medial regions reflect bodily representations and exhibit only modest evoked activity to whisker stimulation (Chapin and Lin, 1984). Column-normalized PDC did not show significantly more cS1 driving to e2 than to e3, nor did it indicate that driving to e6 was significantly larger than driving to e5. The other methods did show significantly more driving to e2 and e6 than to e3 and e4 respectively. Table 3 lists the effect sizes of these comparisons per method. All methods distinguished targets of cS1 with medium to large effect sizes.

At the peak latencies of cS1 driving, row- and column-wise normalized methods suggested different patterns of driving from cS1 to ipsilateral cortex (Fig. 4). Column-wise normalized methods suggested considerable, undifferentiated driving to ipsilateral cortex, with large

variability across animals. Row-wise normalized methods indicated more specific driving to ipsilateral cortex, with smaller 95% CIs. Row-wise normalized PDC suggested that cS1 specifically targets e14, while DTF and wDTF suggested predominant targeting of e10. These regions receive transcallosal monosynaptic connections from cS1 and are the homotopic regions of the main contralateral S1 targets (e6 and e10).

After the initial peak latencies, each method showed qualitatively different dynamics of driving (Fig. 3). Column-normalized PDC values increased during the early period until about 20 ms and then stayed relatively constant at middle (>20 ms) and longer latencies (>40 ms; Fig. 3A). These dynamics reflect the column-wise normalization which bounds the sum of the outgoing PDC plus the autoregressive part to one. For row-normalized PDC and DTF dynamics of summed outflow depended on channel (Fig. 3B–C). Electrode e4 (cS1, green) and e2 (dark blue) decreased their driving at longer latencies while others stayed relatively constant (e.g. e7, red) or showed a continuous increase (e.g. e8, black). Such dynamics are unlikely to be physiologically correct.

Column-normalized wPDC showed sustained driving from e4 (cS1) and e2 at middle latencies (Fig. 3C), yet there is little activity in cS1 at these latencies and hence no mechanism for it to exert influence on other areas (Quairiaux et al., 2011). At longer latencies, column-normalized wPDC did show decreased driving from cS1, in line with physiology, while ipsilateral S1 (iS1, green dotted line) became the largest driver. Driving from iS1 at middle latencies seems plausible since iS1 shows activity at those latencies (Quairiaux et al., 2011; Shuler et al., 2001). At longer latencies, however, iS1 activity falls off and predominant iS1 driving seems less likely. Row-normalized wPDC showed more plausible and better articulated dynamics (Fig. 3D). Whereas cS1 was the main driver at early latencies, iS1 became the largest driver at middle latencies, with mean peak driving latency at 25.7 ms (95% CI 20.0–33.9 ms across animals) that matched the peak latency of the SEP over iS1 (29 ms, 95% CI 26.5–31.4 ms). wDTF showed similar dynamics, with peak iS1 driving latency at 26.9 ms (95% CI 20.3–37.9 ms).

Table 3
Effect sizes (*d*) for distinguishing cS1 and iS1 targets for each method.

	cS1 targets		iS1 targets	
	e2 > e3	e6 > e5	e10 > e11	e14 > e13
Col PDC	1.0	0.6	0.6	0.2
Col wPDC	1.0	0.9	0.4	0.3
Row PDC	0.8	0.6	0.8	0.9
Row wPDC	0.7	0.5	0.3	0.6
DTF	0.9	0.4	0.6	0.1
wDTF	0.7	0.3	0.1	0.02

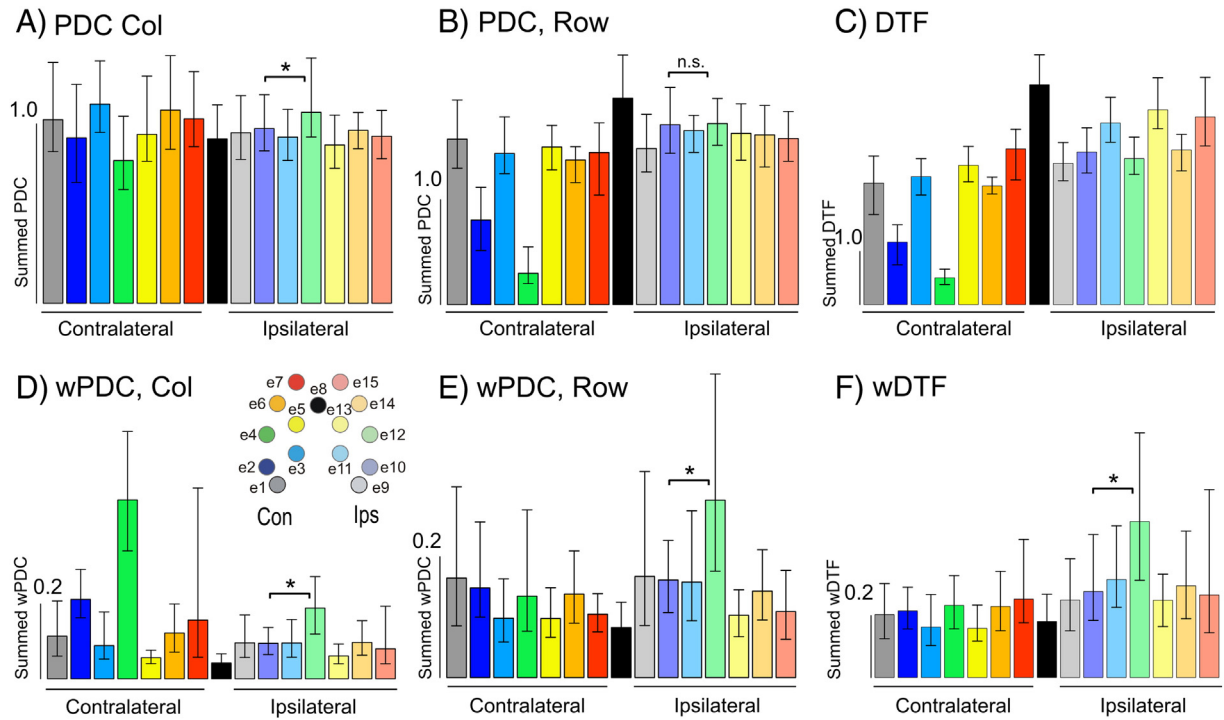


Fig. 5. Identification of iS1 as an important network driver. Average summed driving for each of the six methods is plotted at 26 ms after whisker stimulation. Error bars denote 95% CI around the mean.

The driving role for iS1 as shown by wPDC and wDTF has to our knowledge not been previously demonstrated. We therefore asked whether the other methods showed indications that ipsilateral S1 as an important driver around this latency (26 ms). All methods except row-normalized PDC and DTF, identified iS1 as the largest ipsilateral driver (Fig. 5). We statistically compared summed driving from e12 (iS1) to that of e10, which was among the largest ipsilateral drivers for each method. For these comparisons the largest effect sizes were

obtained with wPDC ($d = 0.8$ and 0.7 for column- and row-wise normalized wPDC, respectively) and wDTF ($d = 0.7$), as compared to PDC ($d = 0.3$ and 0.02 for column- and row-wise normalization respectively).

At these middle latencies, column normalized wPDC (Fig. 3D) furthermore indicated strong driving from cS1, which seems unlikely since spiking activity is absent at this latency and current sinks are feeble (Quairiaux et al., 2011).

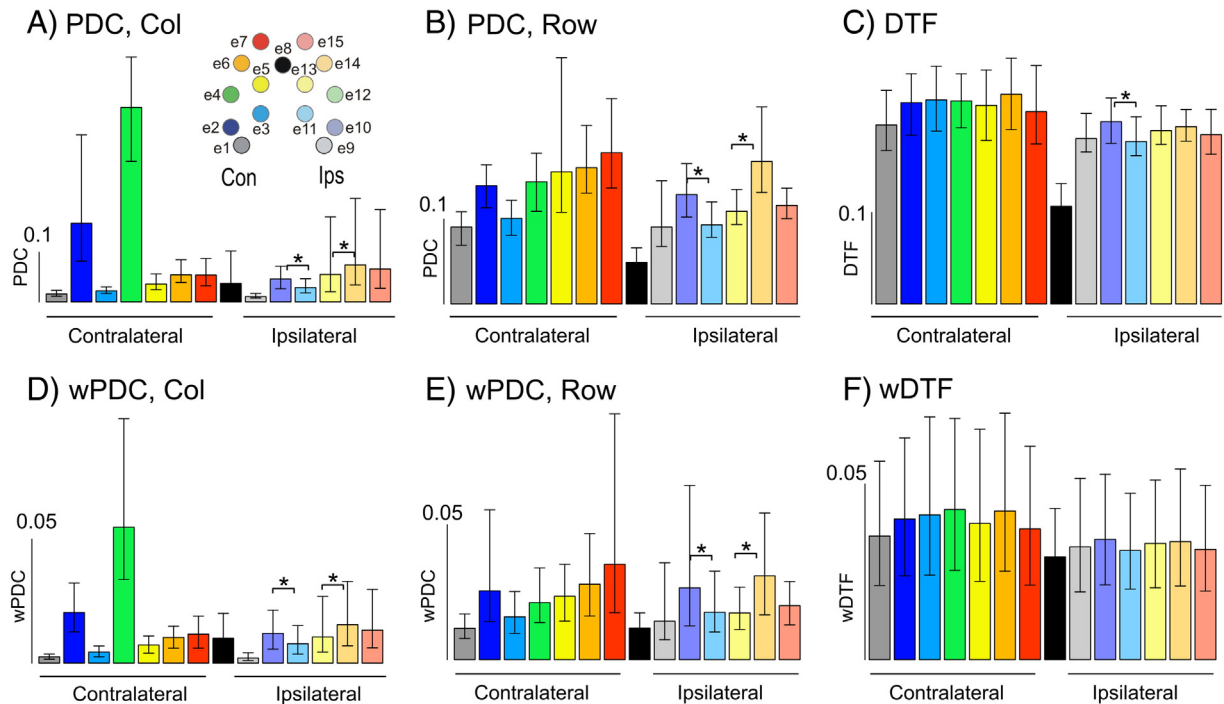


Fig. 6. Directions of driving from ipsilateral S1. Barplots show for each method the driving from iS1 to all target regions in the hemisphere contralateral and ipsilateral to stimulation. Barplots are drawn at 26 ms, corresponding to the peak latencies of iS1 in Fig. 1. Error bars denote 95% CI around the mean.

Given that iS1 appears to be an important driver we next asked what the main targets of iS1 driving are within the ipsilateral hemisphere. If results follow the physiology, similar target are expected for iS1 as for cS1, namely e14 and e10 which cover the homotopic regions of the main targets of cS1 driving (e2, e6; see Fig. 4). The four PDC methods identified e14 and e10 as the main ipsilateral targets of iS1 driving, whereas DTF only distinguished e10 and wDTF showed no specific targeting of ipsilateral regions (Fig. 6). We statistically compared the driving from iS1 (e12) to e10 and e14 with that toward medial electrodes equidistant from iS1, e11 and e13 respectively, as done for cS1. The PDC methods confirmed significantly more driving to e10 and e14 but with medium to large effect sizes (Table 3), whereas DTF only reliably distinguished e10 from e11 and wDTF did not distinguish targets from iS1.

The characterization of driving from iS1 back to contralateral cortex depended on the normalization used (Fig. 6), and not on weighting by the PSD. Whereas column-normalized PDC results indicated large driving back to e4 (cS1) and e2, row-normalized PDC suggested additional driving towards contralateral frontal regions (e6–e7), while DTF suggested large, undifferentiated driving back to the contralateral hemisphere.

Discussion

Using multi-electrode cortex-wide SEP recordings in rats we evaluated the physiological plausibility of time-varying connectivity results obtained with several Granger-causal methods. We compared the effects of row- and column-wise normalization and the effects of weighing by the PSD according to three performance criteria. Most methods correctly identified cS1 as the main driver of the network at early latencies, coinciding with considerable neural activity in cS1. However, PSD weighting allowed for better discrimination of the major drivers (larger effect sizes), and row-wise normalization increased the precision of peak driving latencies. Row-wise normalized methods also more plausibly reflected the initial targets of cS1 driving than column-wise normalization. In sum, results obtained with row-normalized wPDC and wDTF are in better correspondence with what is expected from physiology than results from the other methods. Importantly, only row-normalized wPDC and wDTF results never contradicted known physiology.

PDC can be considered as a factorization of the Directed Coherence, derived using either a column- or row-wise normalization (Baccalá and Sameshima, 2001; Baccala et al., 1998). A column-wise normalization bounds the *outgoing* PDC values to unit and therefore the strength of each outgoing PDC is co-determined by the others to some degree: an increase in the strength of (non-normalized) PDC directed from one driving area to any target areas will reduce the other PDC values outgoing from this driving area. A row-wise normalization bounds the *incoming* connectivity values to a region, which is how DTF is normalized. This way, the value of each incoming connection strength is co-determined by the others: when the strength of influence from one region to a target region increases, the connectivity values from the other regions targeting the same area will appear smaller. This is in line with the interpretation of PDC as a rate of change (Schelter et al., 2009) and makes row-wise normalized PDC better interpretable than column-wise normalized PDC. Moreover, row-wise normalization has the advantage that it allows for more variability in the *outgoing* connectivity strengths because they remain unbounded. The sum of outgoing PDC (outflow) is of particular interest in neural systems, as it allows to identify the main sources of information in the network. Several alternative normalizations exist in the literature (Baccala et al., 2007; Lin et al., 2009; Schelter et al., 2009). By directly comparing the performance of column- and row-wise normalized methods in real data we found that row-wise normalized methods provide a better characterization of the directional selectivity of cS1 driving, in particular to ipsilateral cortex (Fig. 5B, D). Whereas column-wise normalization suggested

large and undifferentiated driving from cS1 to ipsilateral cortex (Fig. 4A, C), row-normalized results suggest that cS1 driving to ipsilateral cortex does not exceed cS1 driving to contralateral cortex, and that cS1 specifically targets ipsilateral frontal sensory-motor region (e14). This is physiologically more plausible than the column-normalized results because e14 is the homologue of the main target of cS1 in contralateral cortex and S1 has structural connections to this region in both hemispheres (Colechio and Alloway, 2009). Although DTF results showed relatively large driving to ipsilateral cortex, it was specifically directed to physiologically plausible areas: ipsilateral parietal and primary sensory regions.

By comparing the two normalizations we also found better temporal resolution for row- than column-wise normalized methods. Row-normalized methods identified peak driving latencies with 95% CIs that were twice as small as those from column-normalized methods, in good agreement with the small variability observed in ERP peak latencies. Column-wise normalization may reduce temporal resolution because it limits the sum of outgoing connection strengths from a channel plus its autoregressive part to one, at every time point. For analysis we did not take the autoregressive part into account when summing the driving from a channel, but this normalization still severely constrained the temporal variations. This can be seen from the dynamics of summed column-normalized PDC (Fig. 3A), which show persistent driving from all regions at latencies beyond 20 ms with little temporal variations. The low values in the first 20 ms indicate that each channel has large autoregressive parts, i.e. that each region is more or less self-determined. At longer latencies, network interactions increase and the autoregressive parts become less important, resulting in persistently high values of summed outgoing PDC.

Nonetheless, column-normalized results often qualitatively agreed with row-normalized results. For example, both normalizations correctly identified the main contralateral targets of cS1 driving, and column-wise results even showed somewhat better discriminability here. In addition, column-normalized PDC has been successfully applied previously (Astolfi et al., 2008; Baccalá and Sameshima, 2001; Hesse et al., 2003; Möller et al., 2001; Takahashi et al., 2010). Yet when the goal is to study dynamic interactions in neural systems, a good temporal resolution is highly desirable and our findings indicate that a row-wise normalization is preferred in this respect.

Although row-wise normalized PDC and DTF frequently gave comparable results, DTF performed poorly in detecting cS1 as a major driver (criterion 1). Instead, it indicated large driving from two neighboring areas (e2 and e3, Fig. 3C), suggesting that driving from these areas is similar to or exceeds that from cS1 at early latencies. The inability to distinguish between these neighboring areas may result from how DTF reflects both direct and indirect driving toward other areas. When weighted by the spectral power, however, cS1 detection performance was comparable to that of row-normalized wPDC, showing that spectral weighting is beneficial for DTF.

The theoretical motivation for weighting by the PSD is to make the results better interpretable. The weighting implements the idea that neural activity is necessary but not sufficient in order for one region to change activity in another region, in line with the interpretation of PDC as a rate of change (Schelter et al., 2009). The wPDC takes the activity in a region into account, but with independent normalizations of PDC and PSD to assure that they can equally contribute. This normalization ensures that wPDC tends to zero when PDC tends to zero irrespective of PSD, and vice versa. This way regions can be active without influencing others. The same holds for wDTF, which was defined analogously to wPDC.

Two previously defined methods also incorporate spectral power in the quantification of directed interactions. Information PDC (iPDC, Takahashi et al., 2010) weights the PDC from j to i by the spectral density of the partialized model process associated with time series j , given the remaining time series. This produces a scale-invariant quantity of connectivity that falls entirely within the framework of information theory.

This has the benefit that iPDC values can be easily interpreted and compared between groups and studies. A spectral scaling of DTF using the PSD of the MVAR model has been previously proposed to better identify dominant frequencies of interaction and localize the foci of epileptic seizures (Van Mierlo et al., 2011, 2013).

To estimate PSD from the signal we used the S-transform (Stockwell et al., 1996). Time-frequency analysis is a trade-off between temporal and spectral resolution and different methods optimize this trade-off in different ways. However, we don't expect that results from wPDC will be qualitatively different when using alternative methods for calculating PSD (e.g. a wavelet-based approach). Although time-frequency transforms have limited temporal resolution with respect to the original signal, our data show that PSD-weighted results have sufficient temporal resolution to distinguish the dynamics of driving in large-scale networks.

We calculated PSD and PDC for frequencies in the 1–150 Hz range, but we only selected the frequencies of maximal PSD for further analysis. This data-driven selection does justice to the observation that electrodes showed different spectral content (Fig. 1C, D) and avoids pre-selecting a specific frequency or frequency band for analysis. In addition, the frequency of maximal activity is the best candidate for driving toward another region. However, the selection risks that some driving may be missed at frequencies that are not as strongly expressed. We chose a reduction of dimensionality in the frequency domain over a full investigation of effects across different frequency bands because the aim of the current work was to illustrate how a benchmark dataset can distinguish between different time-varying connectivity methods.

Our results indicate two specific advantages for weighting by PSD, irrespective of normalization. The first advantage is that major drivers can be more clearly identified. Compared to PDC, the effect sizes from wPDC were more than four times as large for identifying cS1 as the first major driver. For DTF spectral weighting was needed to detect cS1. The PSD reproduces physiological observations, and weighting by PSD takes these physiological observations into account to quantify the influence of one region on another. Yet the clear cS1 identification is not only due to the weighting: wPDC can only be high when both PSD and PDC are high, since each is normalized before multiplication. The same holds for wDTF. That the PSD is not all-determining can be seen e.g. from the driving of e7. At around 20 ms this contralateral frontal-most electrode has the highest amplitude (red trace in Fig. 1), yet scaling by the spectral power does not make it stand out as one of the main drivers (Fig. 3).

The second advantage of weighting by the PSD is that it provides a more plausible dynamics of driving, irrespective of normalization. For example, the dynamics of row-normalized PDC showed continuous increases in several channels that are unlikely to be physiologically correct (Fig. 4B). These progressive increases occurred in channels with little activity at longer latencies and may reflect unstable PDC results obtained from channels with low SNR (Fasoula et al., 2013). In our data DTF showed similar progressive increases, suggesting that the problem may have to do with the MVAR model, rather than in the normalization used. Weighting by the PSD resulted in a highly plausible and interesting dynamics of driving (Fig. 3D). In addition, it revealed that ipsilateral S1 may be an important driver at middle latencies.

The finding that ipsilateral S1 plays a driving role in the middle parts of the sensory evoked response was confirmed by most methods used here. That iS1 is an important driver has to our knowledge not been previously suggested but is in line with iS1 activity observed at these latencies and known functional interactions between ipsi- and contralateral S1 (Shuler et al., 2001a). In our data, driving from iS1 predominantly targets the same regions in ipsilateral cortex as cS1 targets in contralateral cortex, as suggested by all methods with medium to large effect sizes. This is in good agreement with known structural connectivity of S1 (Colechio and Alloway, 2009; Hoffer et al., 2003; Lee et al., 2011; Smith and Alloway, 2013; Zakiewicz et al., 2011).

The main targets of driving from iS1 back to contralateral cortex were not unambiguously identified. Whereas column-normalized

methods suggested contralateral S1 and parietal areas (e2) as the main targets, row-normalized methods identified additional frontal areas as targets (Fig. 6). S1 projects to sensory and sensory-motor areas in the other hemisphere (Colechio and Alloway, 2009; Smith and Alloway, 2013), but to what extent these connections are functionally used is not known. Both scenarios are in line with an active role for iS1 in the bilateral integration of sensory information, as well as the coordination of motor responses (Aronoff et al., 2010; Matyas et al., 2010; Shuler et al., 2001). The finding that iS1 is an important network driver predicts that silencing iS1 will change the middle and later part of the SEP, and this could be experimentally tested. For such a test column-normalized results predict that the later part of the cS1 response will be most strongly affected by iS1 silencing, whereas row-normalized result predicts that activity over contralateral frontal regions will be most affected.

Electrophysiological recordings reflect not only neural activity from nearby tissue but also activity from further away due to instantaneous volume conduction (Gómez-Herrero et al., 2008; Haufe et al., 2013; Nolte et al., 2004; Nunez and Srinivasan, 2006). Volume conduction can make connectivity results hard to interpret (Haufe et al., 2013). When an EEG channel shows strong driving, it is not necessarily the neural tissue immediately underneath that does this driving. The interpretability crucially depends on how uniquely the signals reflect local activity. For example, interpretability is worse for connectivity analyses of scalp EEG than for source estimates (Gómez-Herrero et al., 2008; Supp et al., 2007). In our SEP data, volume conduction effects do not seem to be problematic. The signals in each electrode are highly location-specific (Fig. 1) because rodent cortex is essentially flat (lissencephalic). Furthermore, the SEP signals correspond well to intracranial data recorded immediately underneath (Armstrong-James et al., 1992; Mégevand et al., 2008; Quairiaux et al., 2011). The location-specificity of the signals is furthermore corroborated by the good detection of cS1 as the major driver for almost all methods used, as well as good discrimination of the main targets of cS1.

Within the framework of Wiener–Granger causality there exist numerous alternative methods to estimate directed relations between neurophysiological signals (e.g. Barnett and Seth, 2014; Barrett et al., 2010; Dhamala et al., 2008; Geweke, 1982, 1984; Lin et al., 2009; Roelstraete and Rosseel, 2012), including non-linear approaches (Granger, 2008; Marinazzo et al., 2008). From the large number of published methods a “gold standard” has yet to emerge. Each method has theoretical advantages and disadvantages and we therefore consider direct comparisons on real data with known physiology an important step in establishing a standard. We here focused on a limited number of time-varying methods to demonstrate the feasibility of testing for physiological plausibility using rat SEPs, and to allow for a direct comparison of the effects of different normalizations and weighting by the spectral power. Our work followed the original PDC and DTF definitions (Baccalá and Sameshima, 2001) and the sub-optimal performance of these methods may be improved using alternative definitions. The performance of DTF may be improved by using more recently proposed variants (e.g. Korzeniewska et al., 2003). Similarly, PDC performance may be improved using generalized PDC (gPDC), which normalizes both the numerator and denominator to the variance of the input terms to achieve scale invariance, making it more robust against amplitude differences in the modeled time series (Baccalá et al., 2007). Renormalized PDC (Schelter et al., 2009; Sommerlade et al., 2012) is another optimization of the PDC that specifically allows for an interpretation of the results in terms of coupling strength between neural signals. Another measure with good physiological interpretability is Directed Coherence (Baccalá et al., 1998), which quantifies the amount of spectral power change in the target region accounted for by the source region. A limitation of DC is that it does not distinguish direct from indirect connectivity, and results may thus not accurately reflect underlying physiology.

The method used here are all based on MVAR modeling, which requires selecting a model order parameter: the duration taken into account for determining relations between signals. We used Akaike's Information Criterion to find an optimal model order that avoids overfitting in a data-driven way (Bressler and Seth, 2011; Hesse et al., 2003). Importantly, model orders were identical for all methods used so that differences in results cannot be attributed to differences in model order.

Time-varying MVAR approaches are developed to correctly model non-stationary signals and a range of approaches exist, for example Kalman filtering (Hu et al., 2012; Milde et al., 2010), window-based approaches (Ding et al., 2000; Wilke et al., 2008) and state-space modeling (Sommerlade et al., 2012). Here we used adaptive MVAR modeling based on the RLS algorithm (Astolfi et al., 2008; Hesse et al., 2003; Möller et al., 2001). The RLS algorithm uses an adaptation constant (Möller et al., 2001) which has to be chosen in advance. This value may be set between 0.01 and 0.04 with large numbers of repetitions and reasonable SNR (Astolfi et al., 2008). Reducing the constant could increase the accuracy of the models and reduce the sensitivity to noise, but at the cost of temporal resolution (Astolfi et al., 2008; van Mierlo et al., 2011).

Since a direct comparison of all available time-varying directed connectivity measures is beyond the scope of this paper, we make our SEP dataset freely available at <https://sites.google.com/site/fbmlab/data>. We hope this will contribute to the development and systematic evaluation of different time-varying connectivity measures. When methods show implausible results on this dataset, they should be treated with caution when applied to neurophysiological signals. When a method meets the criteria, its performance can be compared to that of other methods by calculating effect sizes for the critical comparisons. Good performance in this dataset should not be taken to mean that new results can be taken at face-value. Time-varying connectivity results are models of observed variables constructed with the aim to better understand dynamic interactions within functional brain networks (Bressler and Seth, 2011). As with any model, its ultimate value comes from whether it generates new insights and testable hypotheses.

In conclusion, we here showed that the physiological plausibility of time-varying connectivity methods can be evaluated using large-scale SEPs from rats. To our knowledge the results from row-normalized wPDC and wDTF provide the first validation of time-varying connectivity measures in an animal model with well-known structural connectivity along fixed criteria. These methods provide a sensitive tool for understanding brain interactions and generate useful models of the dynamic functional connectivity underlying sensory processing in rat cortex. We expect that future applications of these and other methods will help advance our understanding of how networks of neural activity underlie sensory and cognitive processing, how these networks develop, and how they break down in disease.

Acknowledgments

This work was supported by a Swiss National Science Foundation (PZ00P3_131731) Ambizione grant to GP. We thank H. Witte, W. Hesse and L. Leistriz for providing software enabling AMVAR computation and H. Sperdin for the helpful comments on the manuscript.

References

- Armstrong-James, M., Fox, K., Das-Gupta, A., 1992. Flow of excitation within rat barrel cortex on striking a single vibrissa. *J. Neurophysiol.* 68, 1345–1358.
- Aronoff, R., Matyas, F., Mateo, C., Ciron, C., Schneider, B., Petersen, C.C.H., 2010. Long-range connectivity of mouse primary somatosensory barrel cortex. *Eur. J. Neurosci.* 31, 2221–2233.
- Astolfi, L., Cincotti, F., Mattia, D., Marciani, M.G., Baccala, L.A., Fallani, F.D.V., Salinari, S., Ursino, M., Zavaglia, M., Babiloni, F., 2006. Assessing cortical functional connectivity by partial directed coherence: simulations and application to real data. *IEEE Trans. Biomed. Eng.* 53, 1802–1812.
- Astolfi, L., Bakardjian, H., Cincotti, F., Mattia, D., Marciani, M.G., Fallani, F.D.V., Colosimo, A., Salinari, S., Miwakeichi, F., Yamaguchi, Y., Martinez, P., Cichocki, A., Tocci, A., Babiloni, F., 2007a. Estimate of causality between independent cortical spatial patterns during movement volition in spinal cord injured patients. *Brain Topogr.* 19, 107–123.
- Astolfi, L., Cincotti, F., Mattia, D., Marciani, M.G., Baccala, L.A., de Vico Fallani, F., Salinari, S., Ursino, M., Zavaglia, M., Ding, L., Edgar, J.C., Miller, G.A., He, B., Babiloni, F., 2007b. Comparison of different cortical connectivity estimators for high-resolution EEG recordings. *Hum. Brain Mapp.* 28, 143–157.
- Astolfi, L., Cincotti, F., Mattia, D., De Vico Fallani, F., Tocci, A., Colosimo, A., Salinari, S., Marciani, M.G., Hesse, W., Witte, H., Ursino, M., Zavaglia, M., Babiloni, F., 2008. Tracking the time-varying cortical connectivity patterns by adaptive multivariate estimators. *IEEE Trans. Biomed. Eng.* 55, 902–913.
- Baccalá, L.A., Sameshima, K., 2001. Partial directed coherence: a new concept in neural structure determination. *Biol. Cybern.* 84, 463–474.
- Baccala, L.A., Sameshima, K., Ballester, G.G., Do, V.A.C., Timeo-laria, C., 1998. Studying the interaction between brain structures via directed coherence and Granger causality. *Appl. Signal Process.* 5.
- Baccala, L.A., Sameshima, K., Takahashi, D.Y., 2007. Generalized partial directed coherence, in: 2007 15th International Conference on Digital Signal Processing. Presented at the 2007 15th International Conference on Digital Signal Processing, pp. 163–166.
- Barnett, L., Seth, A.K., 2014. The MVGC multivariate Granger causality toolbox: a new approach to Granger-causal inference. *J. Neurosci. Methods* 223, 50–68.
- Barrett, A.B., Barnett, L., Seth, A.K., 2010. Multivariate Granger causality and generalized variance. *Phys. Rev. E Stat. Nonlinear Soft Matter Phys.* 81, 041907.
- Bressler, S.L., 1995. Large-scale cortical networks and cognition. *Brain Res. Brain Res. Rev.* 20, 288–304.
- Bressler, S.L., Seth, A.K., 2011. Wiener–Granger causality: a well established methodology. *NeuroImage* 58, 323–329.
- Chapin, J.K., Lin, C.S., 1984. Mapping the body representation in the SI cortex of anesthetized and awake rats. *J. Comp. Neurol.* 229, 199–213.
- Cohen, J., 1992. A power primer. *Psychol. Bull.* 112, 155–159.
- Colechio, E.M., Alloway, K.D., 2009. Differential topography of the bilateral cortical projections to the whisker and forepaw regions in rat motor cortex. *Brain Struct. Funct.* 213, 423–439.
- Constantinople, C.M., Bruno, R.M., 2013. Deep cortical layers are activated directly by thalamus. *Science* 340, 1591–1594.
- Dhamala, M., Rangarajan, G., Ding, M., 2008. Analyzing information flow in brain networks with nonparametric Granger causality. *NeuroImage* 41, 354–362.
- Ding, M., Bressler, S.L., Yang, W., Liang, H., 2000. Short-window spectral analysis of cortical event-related potentials by adaptive multivariate autoregressive modeling: data preprocessing, model validation, and variability assessment. *Biol. Cybern.* 83, 35–45.
- Faes, L., Erla, S., Nollo, G., 2012. Measuring connectivity in linear multivariate processes: definitions, interpretation, and practical analysis. *Comput. Math. Methods Med.* 2012.
- Farkas, T., Kis, Z., Toldi, J., Wolff, J.R., 1999. Activation of the primary motor cortex by somatosensory stimulation in adult rats is mediated mainly by associational connections from the somatosensory cortex. *Neuroscience* 90, 353–361.
- Fasoula, A., Attal, Y., Schwartz, D., 2013. Comparative performance evaluation of data-driven causality measures applied to brain networks. *J. Neurosci. Methods* 215, 170–189.
- Florin, E., Gross, J., Pfeifer, J., Fink, G.R., Timmermann, L., 2011. Reliability of multivariate causality measures for neural data. *J. Neurosci. Methods* 198, 344–358.
- Geweke, J., 1982. Measurement of linear dependence and feedback between multiple time series. *J. Am. Stat. Assoc.* 77, 304–313.
- Geweke, J.F., 1984. Measures of conditional linear dependence and feedback between time series. *J. Am. Stat. Assoc.* 79, 907–915.
- Gómez-Herrero, G., Atienza, M., Egiazarian, K., Cantero, J.L., 2008. Measuring directional coupling between EEG sources. *NeuroImage* 43, 497–508.
- Granger, C.W.J., 1969. Investigating causal relations by econometric models and cross-spectral methods. *Econometrica* 37, 424–438.
- Granger, C.W.J., 2008. Non-linear models: where do we go next – time varying parameter models? *Stud. Nonlinear Dyn. Econom.* 12, 1–11.
- Haufe, S., Nikulin, V.V., Müller, K.-R., Nolte, G., 2013. A critical assessment of connectivity measures for EEG data: a simulation study. *NeuroImage* 64, 120–133.
- Hesse, W., Möller, E., Arnold, M., Schack, B., 2003. The use of time-variant EEG Granger causality for inspecting directed interdependencies of neural assemblies. *J. Neurosci. Methods* 124, 27–44.
- Hoffer, Z.S., Hoover, J.E., Alloway, K.D., 2003. Sensorimotor corticocortical projections from rat barrel cortex have an anisotropic organization that facilitates integration of inputs from whiskers in the same row. *J. Comp. Neurol.* 466, 525–544.
- Hu, L., Zhang, Z.G., Hu, Y., 2012. A time-varying source connectivity approach to reveal human somatosensory information processing. *NeuroImage* 62, 217–228.
- Kaminski, M.J., Blinowska, K.J., 1991. A new method of the description of the information flow in the brain structures. *Biol. Cybern.* 65, 203–210.
- Korzeniewska, A., Mańczak, M., Kamiński, M., Blinowska, K.J., Kasicki, S., 2003. Determination of information flow direction among brain structures by a modified directed transfer function (dDTF) method. *J. Neurosci. Methods* 125, 195–207.
- Kus, R., Kaminski, M., Blinowska, K.J., 2004. Determination of EEG activity propagation: pair-wise versus multichannel estimate. *IEEE Trans. Biomed. Eng.* 51, 1501–1510.
- Lee, T., Alloway, K.D., Kim, U., 2011. Interconnected cortical networks between primary somatosensory cortex septal columns and posterior parietal cortex in rat. *J. Comp. Neurol.* 519, 405–419.
- Lin, F.-H., Hara, K., Solo, V., Vangel, M., Belliveau, J.W., Stufflebeam, S.M., Hämäläinen, M.S., 2009. Dynamic Granger–Geweke causality modeling with application to interictal spike propagation. *Hum. Brain Mapp.* 30, 1877–1886.

- Marinazzo, D., Pellicoro, M., Stramaglia, S., 2008. Kernel method for nonlinear Granger causality. *Phys. Rev. Lett.* 100, 144103.
- Matyas, F., Sreenivasan, V., Marbach, F., Wacongne, C., Barsy, B., Mateo, C., Aronoff, R., Petersen, C.C.H., 2010. Motor control by sensory cortex. *Science* 330, 1240–1243.
- Mégevand, P., Quairiaux, C., Lascano, A.M., Kiss, J.Z., Michel, C.M., 2008. A mouse model for studying large-scale neuronal networks using EEG mapping techniques. *NeuroImage* 42, 591–602.
- Milde, T., Leistritz, L., Astolfi, L., Miltner, W.H.R., Weiss, T., Babiloni, F., Witte, H., 2010. A new Kalman filter approach for the estimation of high-dimensional time-variant multivariate AR models and its application in analysis of laser-evoked brain potentials. *NeuroImage* 50, 960–969.
- Möller, E., Schack, B., Arnold, M., Witte, H., 2001. Instantaneous multivariate EEG coherence analysis by means of adaptive high-dimensional autoregressive models. *J. Neurosci. Methods* 105, 143–158.
- Nolte, G., Bai, O., Wheaton, L., Mari, Z., Vorbach, S., Hallett, M., 2004. Identifying true brain interaction from EEG data using the imaginary part of coherence. *Clin. Neurophysiol.* 115, 2292–2307.
- Nunez, P.L., Srinivasan, R., 2006. *Electric Fields of the Brain: The Neurophysics of EEG*. Oxford University Press.
- Porcaro, C., Coppola, G., Pierelli, F., Seri, S., Di Lorenzo, G., Tomasevic, L., Salustri, C., Tecchio, F., 2013. Multiple frequency functional connectivity in the hand somatosensory network: an EEG study. *Clin. Neurophysiol.* 124, 1216–1224.
- Quairiaux, C., Mégevand, P., Kiss, J.Z., Michel, C.M., 2011. Functional development of large-scale sensorimotor cortical networks in the brain. *J. Neurosci. Off. J. Soc. Neurosci.* 31, 9574–9584.
- Roelstraete, B., Rosseel, Y., 2012. Does partial Granger causality really eliminate the influence of exogenous inputs and latent variables? *J. Neurosci. Methods* 206, 73–77.
- Schelter, B., Timmer, J., Eichler, M., 2009. Assessing the strength of directed influences among neural signals using renormalized partial directed coherence. *J. Neurosci. Methods* 179, 121–130.
- Shuler, M.G., Krupa, D.J., Nicolelis, M.A.L., 2001. Bilateral integration of whisker information in the primary somatosensory cortex of rats. *J. Neurosci.* 21, 5251–5261.
- Smith, J.B., Alloway, K.D., 2013. Rat whisker motor cortex is subdivided into sensory-input and motor-output areas. *Front. Neural Circuits* 7.
- Sommerlade, L., Thiel, M., Platt, B., Plano, A., Riedel, G., Grebogi, C., Timmer, J., Schelter, B., 2012. Inference of Granger causal time-dependent influences in noisy multivariate time series. *J. Neurosci. Methods* 203, 173–185.
- Stockwell, R.G., Mansinha, L., Lowe, R.P., 1996. Localization of the complex spectrum: the S transform. *IEEE Trans. Signal Process.* 44, 998–1001.
- Supp, G.G., Schlögl, A., Trujillo-Barreto, N., Müller, M.M., Gruber, T., 2007. Directed cortical information flow during human object recognition: analyzing induced EEG gamma-band responses in brain's source space. *PLoS ONE* 2, e684.
- Takahashi, D., Baccalá, L., Sameshima, K., 2010. Information theoretic interpretation of frequency domain connectivity measures. *Biol. Cybern.* 103, 463–469.
- Van Mierlo, P., Carrette, E., Hallez, H., Vonck, K., Van Roost, D., Boon, P., Staelens, S., 2011. Accurate epileptogenic focus localization through time-variant functional connectivity analysis of intracranial electroencephalographic signals. *NeuroImage* 56, 1122–1133.
- Van Mierlo, P., Carrette, E., Hallez, H., Raedt, R., Meurs, A., Vandenberghe, S., Van Roost, D., Boon, P., Staelens, S., Vonck, K., 2013. Ictal-onset localization through connectivity analysis of intracranial EEG signals in patients with refractory epilepsy. *Epilepsia* 54, 1409–1418.
- Wilke, C., Ding, L., He, B., 2007. An adaptive directed transfer function approach for detecting dynamic causal interactions. Presented at the 29th Annual International Conference of the IEEE Engineering in Medicine and Biology Society, 2007. EMBS 2007, pp. 4949–4952.
- Wilke, C., Ding, L., He, B., 2008. Estimation of time-varying connectivity patterns through the use of an adaptive directed transfer function. *IEEE Trans. Biomed. Eng.* 55, 2557–2564.
- Zakiewicz, I.M., van Dongen, Y.C., Leergaard, T.B., Bjaalie, J.G., 2011. Workflow and atlas system for brain-wide mapping of axonal connectivity in rat. *PLoS ONE* 6, e22669.